Liquid Crystals
Publication details, including instructions for authors and subscription information:
http://www.informaworld.com/smpp/title~content=t713926090

Neutron reflectivity studies of the interface between a small molecule liquid crystal and a polymer

Gary W. Lynn; M. D. Dadmun; Wen-Li Wu; Eric K. Lin; William E. Wallace

Online publication date: 11 November 2010

To cite this Article Lynn, Gary W. , Dadmun, M. D. , Wu, Wen-Li , Lin, Eric K. and Wallace, William E.(2002) 'Neutron reflectivity studies of the interface between a small molecule liquid crystal and a polymer', Liquid Crystals, 29: 4, 551 — 557
To link to this Article: DOI: 10.1080/02678290110120867
URL: http://dx.doi.org/10.1080/02678290110120867

LIQUID CRYSTALS, 2002, VOL. 29, NO. 4, 551–557

Taylor & Francis
Taylor & Francis Group

Neutron reflectivity studies of the interface between a small molecule liquid crystal and a polymer

GARY W. LYNN, M. D. DADMUN*
Department of Chemistry, University of Tennessee, Knoxville, Tennessee 37996-1600, USA

WEN-LI WU, ERIC K. LIN and WILLIAM E. WALLACE
Polymers Division, National Institute of Standards and Technology, 100 Bureau Drive, Gaithersburg, Maryland 20899-8541, USA

(*Received 15 December 2000; in final form 31 August 2001; accepted 30 September 2001*)

In this report, we elucidate the structure of a small molecule liquid crystal/polymer interface using specular neutron reflectivity. More specifically, we have examined the interfacial transition zone width of a small molecule liquid crystal/polymer sample as a function of increasing temperature. The interface between a thin film (≈1000 Å thick) of the liquid crystal 4′-*n*-octyl-4-cyanobiphenyl (8CB) and a thin film (≈800 Å thick) of deuterated poly(methyl methacrylate) (d-PMMA) is broad and broadens with increasing temperature; it was also observed that the thin film geometry influences the mixing behaviour of the 8CB/d-PMMA system. These results may have implications for current theories of liquid crystal display devices formed by the phase separation of liquid crystal polymer mixtures.

1. Introduction

Important areas of liquid crystal display (LCD) technology include the use of polymer stabilized liquid crystals and polymer dispersed liquid crystals (PDLCs) [1]. PDLC systems typically consist of five to ten wt % of liquid crystal dispersed homogeneously in a cross-linked polymer matrix. The confined liquid crystal droplets reside in cavities formed during the polymerization process. In the absence of an electric field, the directors of the liquid crystal are randomly oriented and the material is opaque due to the difference between the refractive indices of the matrix and droplets. When an electric field is applied, the directors align themselves to a preferred orientation and the material becomes transparent if the refractive index of the matrix and effective refractive index of the liquid crystal are very similar. Since PDLC materials exhibit a large surface to volume ratio, surface, rather than bulk, properties dominate the optical characteristics of the device. The specific nature of the liquid crystal/polymer interface controls the surface induced orientation of the liquid crystal, a parameter that affects the ultimate optical properties of the display device. Even though the nature of the liquid crystal/polymer interface strongly influences the optical properties of the resulting structure, there exists very little experimental characterization of these liquid crystal/polymer interfaces.

Numerous experiments have looked at the thermodynamic and structural behaviour of 8CB in confined geometries in order to study liquid crystal interface properties [2]. A few examples of the many experiments include those of Hikmet and Howard who used IR dichroism to examine 8CB in anisotropic gels and plasticized networks [3]. They found that a fraction of the 8CB molecules remained oriented above the nematic to isotropic transition temperatures. A bound fraction of 8CB was largely influenced by the network and did not show a first order nematic to isotropic transition. Iannacchione and Finotello used an a.c. calorimetry technique [4] to measure specific heats of the mesophases of 8CB in Anopore membranes. They concluded that the nematic to isotropic transition strongly depends on the liquid crystal director orientation within an Anopore membrane. Bellini *et al.* and Clark *et al.* have studied 8CB in silica aerogels using light scattering, precision calorimetry and X-ray scattering to show the nematic and nematic to smectic A translational ordering [5, 6]. Their results show that nematic ordering of 8CB in the pores of a silica aerogel does not occur as a first order phase transition like that in the bulk. Experiments on 8CB confined in porous glasses have been conducted by Iannacchione *et al.* via a.c. calorimetry, DSC and

*Author for correspondence; e-mail: dad@utk.edu

Liquid Crystals ISSN 0267-8292 print/ISSN 1366-5855 online © 2002 Taylor & Francis Ltd
http://www.tandf.co.uk/journals
DOI: 10.1080/02678290110120867

small angle neutron scattering as well as by Sinha and Aliev using dielectric spectroscopy [7, 8]. Iannacchione *et al.* showed that for 8CB in a Vycor glass, the nematic to isotropic transition is a continuous transition and not first order. Sinha and Aliev showed that at the nematic to isotropic transition, some degree of orientational order of the 8CB still persists. This result of 8CB in a porous glass is in contrast to that of 8CB in the bulk, where the isotropic phase exists in complete disorder. Finally, Dadmun and Muthukumar [9, 10] have examined the nematic to isotropic transition of liquid crystals in a controlled pore glass and near an adsorbing surface. Both of these studies show the importance of a smooth wall on the orientation of the liquid crystal, as well as the importance of confinement on the order–disorder transition.

In most studies on the interface near liquid crystals, the liquid crystal interface is treated as being very sharp. This treatment is implied in theories ranging from thermodynamic to statistical mechanical and phenomenological approaches [11] which assume that the interface between a liquid crystal and materials such as silica aerogels and porous glasses is sharp. However, this may not be the case for systems where the structure is formed by the phase separation of a liquid crystal and polymer mixture.

Thus, we report in this study information on the structure of the interface between a polymer and small molecule liquid crystal. More specifically, neutron reflectivity has been used to determine the structure of the interface between a small molecule liquid crystal, 8CB and poly(methyl methacrylate). It is hoped that the results presented here will be useful in future experimental and theoretical studies of devices that are formed from small molecule liquid crystal/polymer mixtures. The choice of system was governed by the desire to mimic commercially relevant PDLC or PSLC materials. The cyanobiphenyls, a class of small molecule liquid crystals, is commonly used in PDLC materials. These liquid crystals usually offer nematic to isotropic transitions around room temperature, a transition which becomes important when minimizing the operating voltage. At temperatures farther away from the nematic to isotropic transition, surface anchoring and elastic deformation forces begin to dominate and it becomes increasingly difficult to align the directors of the liquid crystal with an applied electric field.

For our system the small molecule liquid crystal 4′-*n*-octyl-4-cyanobiphenyl (8CB) was chosen. The 8CB transitions include a crystalline to smectic A transition at 21.5°C, a smectic A to nematic transition at 33.5°C and a nematic to isotropic transition at 40.5°C [12]. The acrylates, a class of polymers, are also used extensively in PDLC applications. They typically have refractive indices comparable to those of the small molecule liquid crystals, while ease of crosslinking is another advantage as the structure of crosslinked networks is usually unaffected by temperature or an applied electric field. In our study, deuterated poly(methyl methacrylate) (d-PMMA) has been used as the polymer matrix. The deuteration of the PMMA provides contrast for the neutron reflectivity and d-PMMA is also readily available. One difference from systems used in PDLC or PSLC optical devices is that ours is not crosslinked. Unfortunately, there are many complications and difficulties associated with spin coating a crosslinked thin film polymer, such as ignorance of the degree of crosslinking, and difficulty in forming a uniform sample that is suitable for reflectivity. Thus, we have been unable to complete reflectivity studies on crosslinked d-PMMA.

2. Experimental

A three-layered sample was prepared on a polished silicon wafer (102 mm in diameter, 6 mm thick). As shown in figure 1, the sample consisted of a layer of 8CB on top of the silicon wafer followed by a layer of d-PMMA and topped with a layer of aluminum metal. The silicon wafer ({1 1 1} n-type) was first placed in a buffered etch solution to remove the native oxide layer from the polished surface. The wafer was then placed in a UV/ozone cleaner to remove organic impurities and

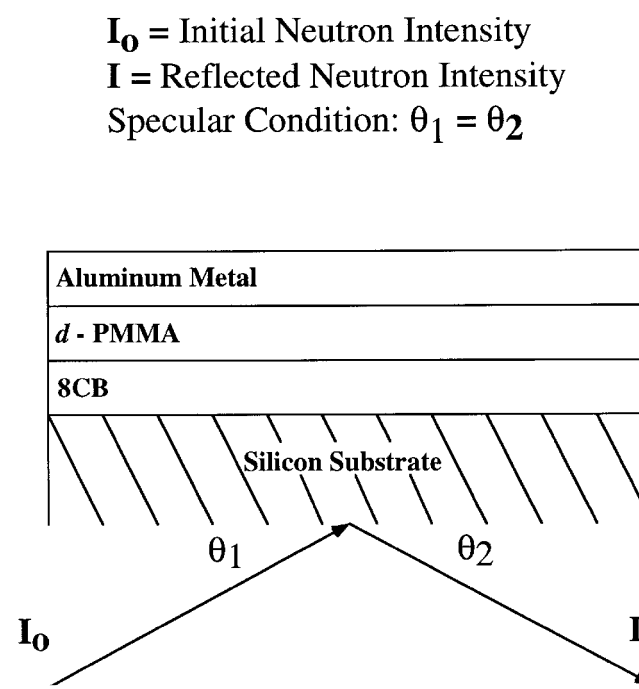

Figure 1. Depiction of the various thin films, their arrangement on the silicon substrate (not drawn to scale), and the incident and reflected neutron beams. The thickness of the 8CB, d-PMMA and aluminum metal are approximately 1000, 800 and 1000 Å respectively.

to regrow a native oxide surface. The 8CB was purchased from Aldrich and used without further purification†. A smectic A to nematic transition and nematic isotropic transition at (33.1 ± 0.2)°C and (40.1 ± 0.2)°C, respectively, were determined using a Mettler Toledo DSC821^e differential scanning calorimeter (DSC)‡. The 8CB was spin-cast onto the silicon wafer from a toluene solution with a 8CB mass fraction of 2 wt %. The sample was covered and placed in a freezer. The d-PMMA ($M_w = 169\,604$ g mol^{-1}, $M_w/M_n = 1.09$) was purchased from Polymer Source Inc. and used as received§. DSC measured a glass transition temperature of (90.66 ± 0.5)°C for this polymer. A glass micro slide (75×50 mm^2) was wiped clean with acetone and then placed in the UV/ozone cleaner. The d-PMMA was spin-cast onto the glass micro slide from an *o*-xylene solution with a d-PMMA mass fraction of 3.5%. The thin film of d-PMMA was then floated onto the 8CB layer from the glass micro slide in 18 MΩ cm chilled water. This two-layer sample was then placed in a desiccator under vacuum and at room temperature overnight. A 1000 Å thick film of aluminum metal was subsequently evaporated on top of the d-PMMA to ensure that none of the 8CB escaped from the system during thermal treatments of the experiment.

Specular neutron reflectivity measurements were performed on the sample at the National Center for Neutron Research (NCNR) NG-7 reflectometer at the National Institute of Standards and Technology in Gaithersburg, MD. The wavelength (λ) of the neutrons was 4.768 Å with a wavelength spread ($\Delta\lambda/\lambda$) of 0.2. The sample was placed on a heating stage in a vacuum-tight chamber. The neutron beam was passed up through the silicon wafer and out the aluminum/vacuum interface (see figure 1). The ratio of reflected intensity to incident beam intensity (reflectivity) was measured from the silicon wafer/8CB interface parallel at grazing incidence angles between 0.11° and 2.6°. The reflectivity is plotted as a function of the neutron momentum transfer normal to the surface of the sample (Q_z), where $Q_z = (4\pi/\lambda)\sin\theta$ and θ is the incident angle. The neutron scattering length density profile normal to the sample surface can then be determined from the measured reflectivity. Furthermore, it is the elastic coherent scattering per unit volume (Q_c^2) which determines this density profile normal to the surface, where $Q_c^2 = 16\pi nb$ and n is the number density of scattering nuclei ($N_A\rho/M$), b is the neutron scattering length, N_A is the Avogadro constant, ρ is mass density of the species and M is the molar mass of the species. The scattering length density profile is calculated from model fits of the measured reflectivity data. The model fits are determined using a recursive multilayer method [13]. It is necessary to fit the data because not unlike conventional diffraction, one cannot know both the amplitude and phase of the reflected beam. Further details concerning the reflectivity technique are available in the literature [14].

3. Results and discussion

The purpose of this work is to determine the width of the interface between the small molecular liquid crystal and the polymer and its response to a change in temperature. Therefore, the reflectivity of the trilayer sample was measured at a series of temperatures. All temperatures reported below are within ±1.0°C. The sample was equilibrated at each temperature for 45 min before measuring the reflectivity; the duration of each measurement was 2 h 15 min. The sample was also kept at a constant pressure of 7.3×10^{-3} Pa during the experiment.

The reflectivity was first measured at 25°C, and then at 50°C and 75°C. This was followed by a second measurement at 75°C to ensure that the sample was stable in the total 3 h period of measurement. Figure 2 shows that these two curves obtained at 75°C are indeed identical and demonstrate that the layered structure may change with temperature, but not in the course of each measurement. A fifth measurement of the reflectivity was made at 110°C. Figure 3 shows the measured reflectivity curves at 25, 50, 75 and 110°C.

Inspection of the reflectivity curves can prove informative regarding the multi-layer structure. The measured reflectivity curve is a convolution of the reflected intensities from the individual interfaces of the 8CB, d-PMMA and Al layers. The spacing of the interference fringes present in the curve is dominated by the thickness of the d-PMMA. The interference fringes at higher Q_z dampen out due to the surface and/or interface roughness. With increasing temperature, these interference fringes dampen out more rapidly at higher Q_z. This may be because the interfaces are broadening with increasing temperature. This aspect of the curve is difficult to discern visually,

†Certain commercial equipment, instruments, or materials are identified in this paper in order to specify adequately the experimental procedure. Such identification does not imply recommendation or endorsement by the National Institute of Standards and Technology, nor does it imply that the materials or equipment identified are necessarily the best available for the purpose.

‡In this publication, the data reported in the text, figures and table are presented along with the standard uncertainty (±) involved in the measurement.

§According to ISO 31-8, the term 'Molecular Weight' has been replaced by 'Relative Molecular Mass', symbol M_r. Thus, if this nomenclature and notation were to be followed in this publication, one would write $M_{r,n}$ instead of the historically conventional M_n for the number average molecular weight, with similar changes for M_w, M_z and M_v, and it would be called the 'Number Average Relative Molecular Mass'. The conventional notation, rather than the ISO notation, has been employed for this publication.

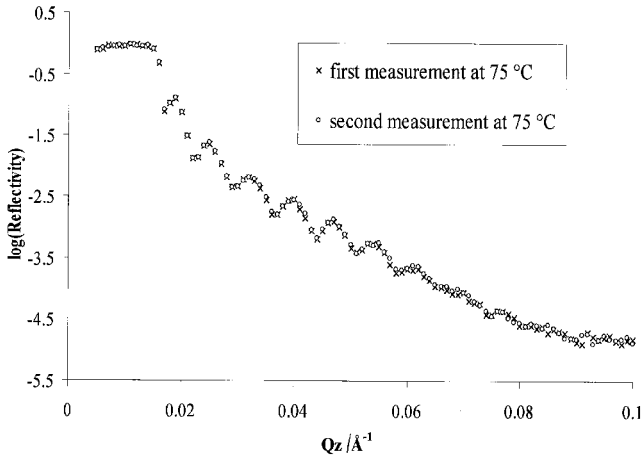

Figure 2. Neutron reflectivity data measured consecutively at 75°C. There appears to be no difference in the two profiles, implying that the reflectivity does not change during the 3 h measurement.

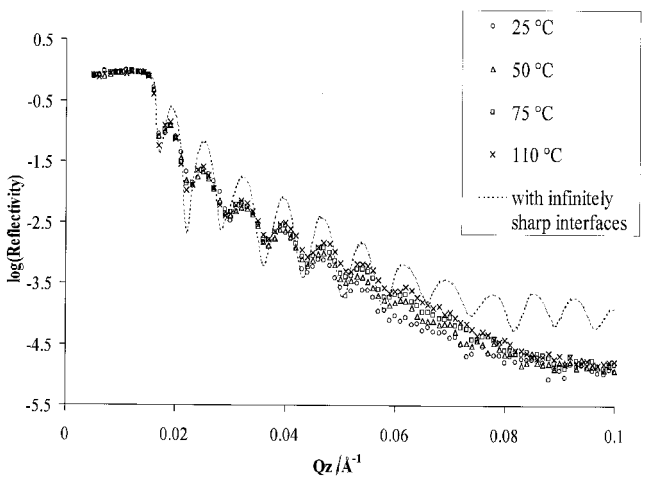

Figure 3. Neutron reflectivity data measured at 25, 50, 75 and 110°C. The dashed curve is the reflectivity profile for a sample with infinitely sharp interfaces and surface.

however these changes can be quantified through the fitting procedure. If the interfaces between the layers were infinitely sharp, the reflectivity curve would follow Porod's Law and decay as Q_z^{-4} [15]; figure 3 also shows a calculated reflectivity profile for our system with infinitely sharp interfaces as the dashed curve. The expected location of a line with Q_z^{-4} dependence would pass through the centre of the dashed curve. However, as can be seen from the comparison of the dashed curve and the experimental data (figure 3), this is not the case for these samples. The curves all fall off more rapidly than the dashed curve, signifying that the interfaces in the sample are not sharp and that there exists a gradient in the scattering length densities between layers. This gradient can be thought of as the transition zone width or roughness between consecutive layers. Thus, this transition zone width between the liquid crystal layer and the d-PMMA is the most significant parameter.

To account quantitatively for the descriptions portrayed in the above paragraph, a model fit was determined for each of the curves in figure 3. Chi-squared values of 1.05, 1.26, 1.21 and 1.44 were obtained for the model fits at 25, 50, 75 and 110°C respectively. Figure 4 shows the model fit and the measured reflectivity curve for the sample at 25°C. The error bars on the experimental data correspond to the standard uncertainty in the measurement. The table shows the result of this fitting procedure for the sample at 25°C. This fit shows that the total thickness for the 8CB thin film is 1023 ± 1 Å. Included in this total thickness are three distinct scattering length density layers; these can be attributed to a layer that is ordered by the silicon surface, a bulk liquid crystal layer, and a layer that is influenced by the d-PMMA interface. The table also shows the thickness and transition zone widths (roughness) of the respective layers. The roughness reported in this table corresponds to that of the previous layer. For example, the roughness of the aligned 8CB layer (5 Å) corresponds to the silicon/aligned 8CB layer interface.

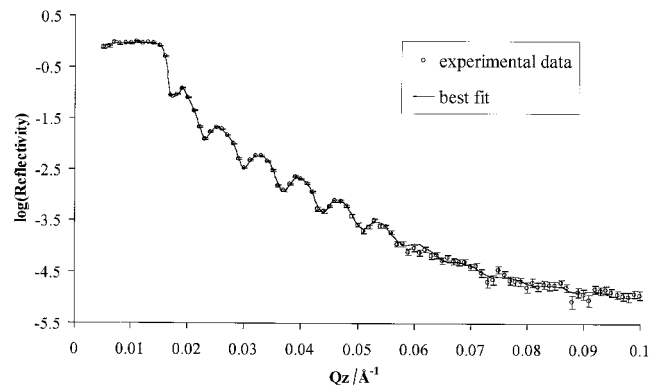

Figure 4. Neutron reflectivity data and best fit for system at 25°C. The error bars indicate the standard uncertainty in the measurement.

Table. Results from the model fitted to the experimental data for the sample at 25°C.

Item	Thickness ± 1/Å	Roughness ± 1/Å
Aligned 8CB layer	110	5
Bulk 8CB layer	631	5
8CB/d-PMMA interface layer	282	328
d-PMMA	785	270
Aluminum metal	869	29
Aluminum oxide	88	61

The data in the table are displayed diagrammatically in figure 5, which shows the scattering length density profile of the sample at 25°C as a function of the layer depth (z) as determined from the fit. As was mentioned earlier, z is normal to the sample surface. Starting at the silicon substrate, one can see an aligned 8CB layer followed by the bulk 8CB layer and then the 8CB/d-PMMA interfacial layer. Inspection of this part of the figure provides some interesting information. The scattering length density of the aligned layer near the Si surface has a greater scattering length density than the bulk layer. This is because the molecules in the ordered layer will be more efficiently packed, producing a system where there are more scattering centres per unit volume, which in turn results in a higher scattering length density.

Interestingly, inspection of figure 5 can lead to the conclusion that there exists a broad interface between the bulk 8CB layer and the d-PMMA layer. However, a fitting of the experimental data to a multilayer system that has a broad interface between the bulk 8CB and the d-PMMA is not sufficient. A suitable fit can only be found if there exists a separate layer between the bulk 8CB and the d-PMMA layer. This result shows that there is a distinct scattering length density layer between the bulk 8CB and the d-PMMA layers, and not just a density gradient. Additionally, of the three layers within the 8CB thin film, this 8CB/d-PMMA interface layer has a higher scattering length density than the aligned and bulk 8CB layers. There are a number of possible interpretations of this fact. One is that it is a very well aligned layer of 8CB. The Q_c^2 of this layer is 1.34×10^{-4} Å^{-2}, as calculated from the model fit of the reflectivity profile. As the Q_c^2 is equal to $16\pi N_A \rho b/M$, the density or neutron scattering length of the layer can be determined from this data. If this layer were pure 8CB, the Q_c^2 value would translate to a mass density of 2.32 g cm^{-3}. This value is much greater than the mass density of 8CB in the smectic A phase, at 27.5°C, which is 1.03 g cm^{-3} [16]. Therefore, this interpretation is not possible, as it would result in a layer that is denser than the bulk 8CB in the crystalline phase. Another possible explanation is that this separate layer is a narrow slice of a one-phase mixture of 8CB and d-PMMA. If this is indeed the case, the composition of this layer can be calculated from:

$$Q_c^2(\text{layer}) = x_1[Q_c^2(\text{8CB})] + x_2[Q_c^2(\text{d-PMMA})],$$
$$(x_1 + x_2 = 1).$$

Here x_1 is the fraction of particles of 8CB scattered in a given volume, x_2 is the fraction of particles of d-PMMA scattered in a given volume, Q_c^2 (8CB) is the scattering length density of the bulk 8CB, and Q_c^2 (d-PMMA) is the scattering length density of the d-PMMA. Using Q_c^2 (layer) $=1.34\times10^{-4}$ Å^{-2}, Q_c^2 (8CB) $=9.67\times10^{-5}$ Å^{-2}, and Q_c^2 (d-PMMA) $=3.37\times10^{-4}$ Å^{-2}, the composition of this interface layer is approximately 93% by mass 8CB and 7% by mass d-PMMA at all temperatures studied. However, inspection of the bulk phase diagram (figure 6) shows that a mixture that is 93% by mass 8CB and 7% by mass d-PMMA will be phase separated for all temperatures below c. 80°C. Therefore, at this time, we are unable to define accurately the physical origin of this interfacial layer. It may be a mixture of an ordered 8CB with d-PMMA, although we are unable to verify this.

It is possible that the origin of this interfacial layer could also be a consequence of the mathematical fitting procedure. However, both an error function and a hyperbolic tangent were used as the functional form to fit the interface, with both functions giving similar results. It is possible that there exists a different functional form that would describe the interface adequately without the interfacial layer, however it is not clear what that would be. Therefore, while the effective interfacial width and Q_c^2

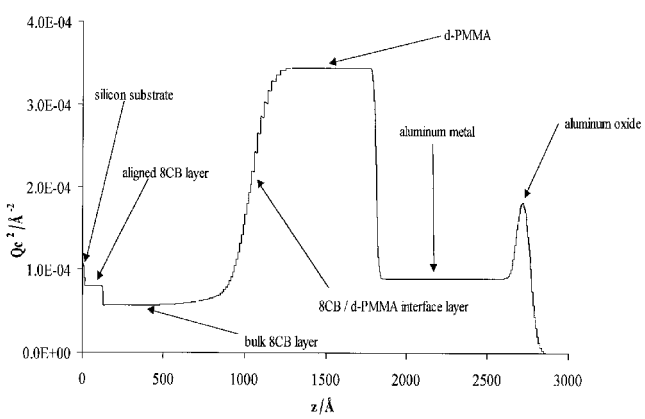

Figure 5. Relative scattering length density as a function of the layer depth (z) for the sample at 25°C.

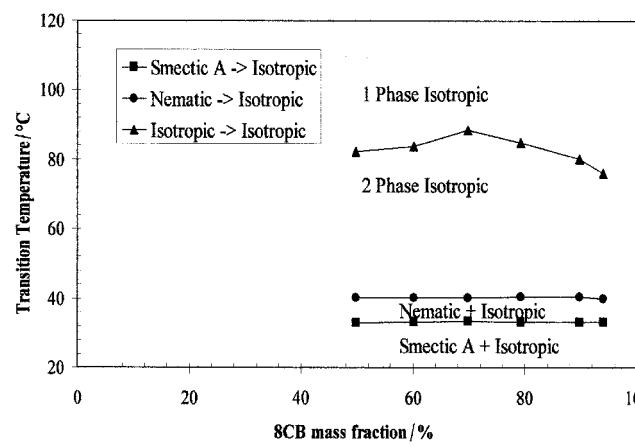

Figure 6. Bulk 8CB/PMMA phase diagram as determined by optical microscopy. The M_w of the PMMA is approximately 120 000 g mol^{-1}.

values obtained for this fitting procedure are quantitative, the functional form describing the interface cannot be proven to be unique. This, however, does not influence the primary conclusions of this paper, as even without the interfacial layer the interface is still quite broad.

The data shown in figures 4 and 5 and the table are for the sample at 25°C. The same model is also utilized to fit the reflectivity data at the other temperatures. Figure 7 shows the scattering length density profiles for the sample at 25, 50, 75 and 110°C. While figure 8 is the same data that has enlarged around the 8CB PMMA interface. These data show the effect of thermal cycling on the 8CB/d-PMMA interface, indicating only slight changes with thermal change. Figure 9 quantifies these changes by plotting the temperature dependence of the

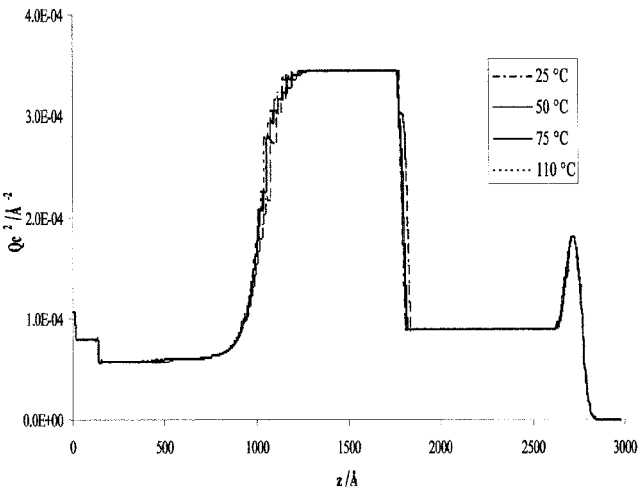

Figure 7. Relative scattering length density as a function of the layer depth (z) for the sample at 25, 50, 75 and 110°C.

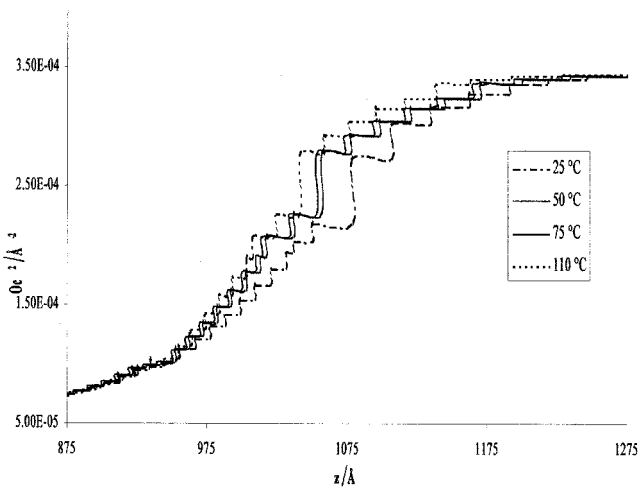

Figure 8. Relative scattering length density as a function of the layer depth 875 Å $< z <$ 1275 Å for the sample at 25, 50, 75 and 110°C.

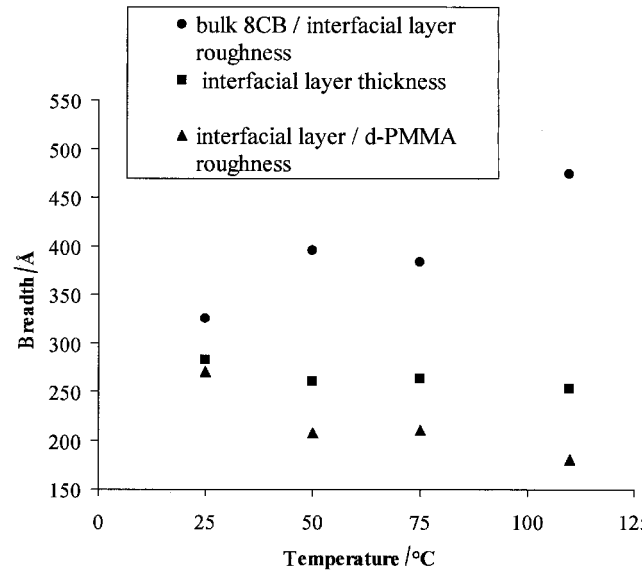

Figure 9. Breadth of the 8CB/d-PMMA interface as a function of temperature. Squares denote the thickness of the interfacial layer; circles denote the roughness of the bulk 8CB/interfacial layer; triangles denote the interfacial layer/d-PMMA roughness.

thickness of the 8CB/d-PMMA interfacial layer as well as of the roughness between this layer and the d-PMMA. This figure demonstrates that the interfacial layer is between 250 and 300 Å and decreases slightly with temperature, while the roughness between the 8CB-rich interfacial layer and the pure d-PMMA decreases from 270 Å at 25°C to 180 Å at 110°C. Figure 9 also shows how the roughness between the bulk 8CB and the interfacial layers varies with increasing temperature: it increases from 325 Å at 25°C to 474 Å at 110°C.

An aim of this work was to quantify the width of the interface between the 8CB and the polymer d-PMMA. From the results described above, there are a number of ways to 'define' this interface. It could be the breadth of the sample between the bulk 8CB and the pure d-PMMA layer. In this case, the interface is on the order of 900 Å and changes only slightly with temperature. If, however, the interfacial width is merely the roughness between the 8CB-rich interfacial layer and the pure d-PMMA, figure 9 shows that this roughness is approximately 300 Å and decreases with temperature. In either definition, it can be stated that the interfacial width between a small molecule liquid crystal and d-PMMA is not sharp.

It is interesting to relate this information, regarding the temperature dependence of the 8CB/d-PMMA interface in a thin film, to the phase behaviour of 8CB and PMMA in the bulk. From a theoretical standpoint, one would expect that the temperature dependence of the interface between two layers would depend on the miscibility of the two components of the layers. If the

two components are miscible in the temperature range of interest, one would expect that an increase in temperature would increase the mobility of the two components and the interface would become broader, until the two layers mix to form one miscible system. On the other hand, if the two components are immiscible in the temperature range, one would expect that the interface would become broader with a decrease in $\Delta H/kT$ of the system, where ΔH is the enthalpy of mixing the two components, k is Boltzmann's constant, and T is the absolute temperature. This decrease in $\Delta H/kT$ correlates to an increase in temperature for a system with an upper critical solution temperature (UCST). Indeed studies of the phase behaviour of cyanobiphenyls with poly(methyl methacrylate) or polystyrene show phase diagrams that exhibit UCST behaviour [17–20]. Thus, the increase in the overall breadth of the LC/PMMA interface with an increase in temperature is understandable merely from the thermodynamics of the mixing process at the 8CB/d-PMMA interface.

However, a more careful inspection of the phase behaviour of 8CB and PMMA elucidates a surprising effect: the 8CB and PMMA are miscible above approximately 80–90°C. The phase diagram of 8CB and PMMA ($M_w = 120\,000$ g mol^{-1}) as determined by DSC and phase contrast microscopy in our lab is shown in figure 6. Clearly, when the multilayer system is brought to 110°C, the bulk system (regardless of composition) is in the miscible region. Therefore, one would expect that the multilayer system would mix to form a single layer of 8CB and d-PMMA at 110°C. However, this is not what is found experimentally. Experiments are continuing in this laboratory to explain this phenomenon and a future publication will expand on its underlying cause.

4. Summary and conclusions

Neutron reflectivity measurements have been completed to evaluate the breadth of the interface between a small molecule liquid crystal and a polymer. The results show that the liquid crystal layer consisting of 8CB that is situated between a silicon surface and a polymer, consists of three distinct scattering density layers. Furthermore, the interface between the liquid crystal and the interface is very broad, on the order of 300–900 Å. The interface also broadens with increasing temperature. One might expect the interfacial broadening to occur at elevated temperatures, but even at a lower temperature of 25°C, the interface is still quite broad. This may have implications for current theories that implicitly treat the interface between a polymer and liquid crystal as a well-defined, sharp interface.

This work was funded by grant No. 70NANB7H0031 from the National Institute of Standards and Technology. Much of this work was done while G.W.L. was a guest researcher in the Electronics Applications Group, Polymers Division, NIST. Therefore, G.W.L. and M.D.D. would like to thank all staff in the Electronics Applications Group for their assistance. The authors would also like to thank Steven C. Roth for help with the evaporation of the aluminum metal, and Nathan Crawford for sharing the data in figure 6.

References

[1] Drzaic, P. S., 1995, *Liquid Crystal Dispersions* (World Scientific).
[2] Crawford, G. P., and Zumer, S. (editors), 1996, *Liquid Crystals in Complex Geometries Formed by Polymer and Porous Networks* (London: Taylor and Francis).
[3] Hikmet, R. A. M., and Howard, R., 1993, *Phys. Rev. E*, **48,** 2752.
[4] Iannacchione, G. S., and Finotello, D., 1992, *Phys. Rev. Lett.*, **69,** 2094.
[5] Bellini, T., Clark, N. A., Muzny, C. D., Wu, L., Garland, C. W., Schaefer, D. W., Olivier, B. J., and Oliver, B. J., 1992, *Phys. Rev. Lett.*, **69,** 788.
[6] Clark, N. A., Bellini, T., Malzbender, R. M., Thomas, B. N., Rappaport, A. G., Muzny, C. D., Schaefer, D. W., and Hrubesh, L., 1993, *Phys. Rev. Lett.*, **71,** 3505.
[7] Iannacchione, G. S., Qian, S. H., Crawford, G. P., Keast, S. S., Neubert, M. E., Doane, J. W., Finotello, D., Steele, L. M., Sokol, P. E., and Zumer, S., 1995, *Mol. Cryst. liq. Cryst.*, **262,** 13.
[8] Sinha, G. P., and Aliev, F. M., 1998, *Phys. Rev. E*, **58,** 2001.
[9] Dadmun, M. D., and Muthukumar, M., 1993, *J. Chem. Phys.*, **98,** 4850.
[10] Dadmun, M. D., and Muthukumar, M., 1994, *J. Chem. Phys.*, **101,** 10 038.
[11] Yokoyama, H., 1997, *Handbook of Liquid Crystal Research*, edited by P. J. Collings and J. S. Patel (Oxford University Press), pp. 179–235, and references therein.
[12] Merck, UK, 1986, product information.
[13] Ankner, J. F., and Majkrzak, C. J., 1992, *Proc. SPIE*, **1738,** 260.
[14] Russell, T. P., 1990, *Mater. Sci. Rep.*, **5,** 171.
[15] Porod, G., 1951, *Kolloid-Z*, **124,** 83; Porod, G., 1952, *Kolloid-Z*, **125,** 51 and 109.
[16] Leadbetter, A. J., Durrant, J. L. A., and Rugman, M., 1977, *Mol. Cryst. liq. Cryst.*, **34,** 231.
[17] Ahn, W., and Kim, C. Y., 1992, *Macromolecules*, **25,** 5002.
[18] Benmouna, F., Daoudi, A., Roussel, F., Buisine, J.-M., Coqueret, X., and Maschke, U., 1999, *J. polym. Sci. B: polym. Phys.*, **37,** 1841.
[19] Benmouna, F., Daoudi, A., Roussel, F., Leclercq, L., Buisine, J.-M., Coqueret, X., Benmouna, M., Ewen, B., and Maschke, U., 2000, *Macromolecules*, **33,** 960.
[20] Crawford, N., and Dadmun, M. D., unpublished results.